Molecular Ionization Dissociation Induced by Interatomic Coulombic Decay in an $ArCH_4$-Electron Collision System

S. Yan, R. T. Zhang, S. Xu, S. F. Zhang, and X. Ma*
Institute of Modern Physics, Chinese Academy of Sciences, Lanzhou 730000, China
and School of Nuclear Science and Technology, University of Chinese Academy of Sciences, Beijing 100049, China

(Received 12 May 2023; revised 11 July 2023; accepted 15 November 2023; published 18 December 2023)

Interatomic Coulombic decay (ICD) is a significant fragmentation mechanism observed in weakly bound systems. It has been widely accepted that ICD-induced molecular fragmentation occurs through a two-step process, involving ICD as the first step and dissociative-electron attachment (DEA) as the second step. In this study, we conducted a fragmentation experiment of $ArCH_4$ by electron impact, utilizing the coincident detection of one electron and two ions. In addition to the well-known decay pathway that induces pure ionization of CH_4, we observed a new channel where ICD triggers the ionization dissociation of CH_4, resulting in the cleavage of the C-H bond and the formation of the CH_3^+ and H ion pair. The high efficiency of this channel, as indicated by the relative yield of the Ar^+/CH_3^+ ion pair, agrees with the theoretical prediction [L. S. Cederbaum, J. Phys. Chem. Lett. **11**, 8964 (2020).; Y. C. Chiang *et al.*, Phys. Rev. A **100**, 052701 (2019).]. These results suggest that ICD can directly break covalent bonds with high efficiency, bypassing the need for DEA. This finding introduces a novel approach to enhance the fragmentation efficiency of molecules containing covalent bonds, such as DNA backbone.

DOI: 10.1103/PhysRevLett.131.253001

The behavior of clusters bound by van der Waals interaction, hydrogen bond, and π-π stacking interaction is distinct from that of an isolated atom, which relaxes its excitation energy only through Auger decay or photon radiation. If one atom (or molecule) A in the cluster is simultaneously ionized and excited, the excess energy from its deexcitation can be transferred to the neighboring atom (or molecule) B, inducing its ionization [1]. This relaxation mechanism is known as Interatomic Coulombic decay (ICD), which has been extensively explored both theoretically and experimentally over the past two decades [2–9]. Many variants of ICD, such as electron transfer mediated decay (ETMD) [10–12] and radiative charge transfer (RCT) [13–15], have also been observed. For further details, please refer to the reviews in [16,17].

ICD and its variants are powerful tools that significantly influence the ionization cross section of an atom (or molecule) B in its neighboring environment. This is because the atom (or molecule) A acts as an antenna, absorbing the energy from radiation or particle collision and passing it on to the receiver atom (or molecule) B. Through this antenna-receiver complex, the single ionization cross section of Ne can be enhanced by more than a factor of 60 [18,19], and the double ionization cross section of Mg can increase by 3 orders [20,21]. Recently, it was discovered that ICD leads to the double ionization of alkali dimers attached to He droplets, with ionization efficiency similar to that in single ionization [22]. Because of this enhancement effect, ICD and its related interatomic processes not only break the AB system via Coulomb explosion but also generate a flood of low-energy electrons and energetic ions in the nanoscale.

It has been demonstrated that low-energy electrons from ICD can cause the rupture of a molecular covalent bond through dissociative electron attachment (DEA) [23–25]. One can use DEA following ICD to break the covalent C—O, P—O, and C—H bonds of the backbone and bases in DNA, leading to the cleavage of DNA double or single strands [26–35]. However, the ICD-DEA mechanism is a two-step process, and its possibility is determined by the probability product of DEA and ICD steps. One may consider whether ICD can directly cause the dissociation of a molecule, rather than via DEA. If this direct dissociation channel is accessible, we anticipate a pioneering approach to enhance the fragmentation efficiency of molecules containing covalent bonds, such as DNA backbone. Recently, Cederbaum [36] and Chiang *et al.* [37] theoretically predicted molecular dissociation by interatomic energy relaxation. For the HeH_2 dimer system, if the He atom is populated into the excitation-ionization state $He^{+*}(2s)$, its decay will trigger the occurrence of ICD (ETMD) and will populate the molecule H_2 into a specific parent state H_2^+ (H_2^{2+}), followed by the dissociation into an H^+/H ion pair (H^+/H^+ ion pair). For the ArN_2 dimer system, using an ICD-like mechanism, the decay following $3s$ electron ionization of the Ar atom leads to the excitation of the N_2 molecule, followed by the breaking into two N atoms [36].

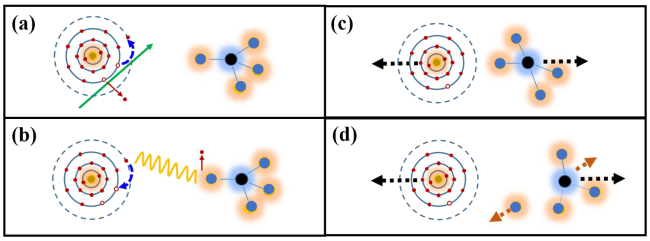

FIG. 1. Reaction sequence observed in the $ArCH_4$ dimer. (a) Incident electron promotes the Ar atom to excitation-ionization states $Ar^{+*}(3p^4\,nl)$. Note the ionization of Ar $3s$ electrons cannot trigger ICD, since the corresponding ionization energy (29 eV) is lower than the ICD threshold energy (32 eV) of the $ArCH_4$ dimer. (b) ICD takes place, the $3p$ vacancy is refilled by nl electrons, and the excess energy is transferred to the CH_4 and ionizes its $1t_2$ electron. (c) Coulomb explosion to Ar^+-CH_4^+ ion pair occurs. The black arrows represent the momenta of the two ions after Coulomb explosion. (d) Dissociation of the CH_4^+ ion to CH_3^+ and H happens. The orange arrows represent the momenta of the two fragments in the center-of-mass frame of the parent CH_4^+ ion.

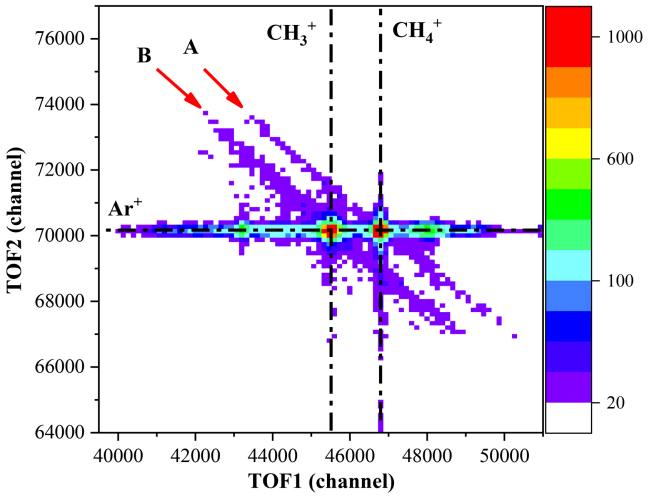

FIG. 2. Two-dimensional TOF correlation map. The arrow marked with A is the Ar^+/CH_4^+ ion pair, while the arrow marked with B is the Ar^+/CH_3^+ ion pair.

In this study, we have experimentally demonstrated that ICD can indeed trigger the cleavage of a covalent bond in a molecule with an efficiency equal to or greater than single ionization by intermolecular energy transfer. The $ArCH_4$ dimer was selected as a prototype system, and the schematic sequence we have observed is illustrated in Fig. 1. First, an incident electron ionizes the Ar atom in the $ArCH_4$ dimer and populates the Ar^+ ion into ionization-excitation states $Ar^{+*}(3p^4nl)$ [Fig. 1(a)]. Then ICD occurs [Fig. 1(b)], causing the ionization of CH_4 and Coulomb explosion to Ar^+-CH_4^+ [Fig. 1(c)]. Finally, the vibrationally excited CH_4^+ ion dissociates into CH_3^+ and H [Fig. 1(d)].

This experiment was conducted using the transversal reaction microscope, modified for dedicated studies of electron impact ionization of molecules and clusters, at the Institute of Modern Physics, Chinese Academy of Sciences [38,39]. The prototype idea for this microscope was proposed decades ago [40,41]. The $ArCH_4$ dimer was produced by adiabatic expansion of the Ar and CH_4 gas mixture with a density ratio of 8:2 in the stagnation of 4 bar. The obtained yield ratio of $ArCH_4$ to Ar atom was about 1%. The incident electron beam with a frequency of 40 kHz, a pulse width of 4 ns, and energy of 480 eV intersected the $ArCH_4$ at the center of the chamber, inducing its ionization and dissociation. The emitted slow electron was accelerated by a weak electric field of 2 V/cm towards the electron position sensitive detector (PSD), while a 4 Gs magnetic field was imposed in the direction of the electric field to increase the collection solid angle of the emitted electron. 400 ns later, the electric field was raised to 30 V/cm to collect the recoil ion by the ion PSD detector. Based on the time of flight (TOF) and position information, we reconstructed the momenta of the ions and electrons after the collision, and obtained these kinetic energy release (KER, sum of the kinetic energy of all charged ions) spectra and electron energy spectra for selected collision events based on electron-ion coincidences. Before this experiment, a fragmentation experiment on Ne_2 was carried out to calibrate our setup. For the sum of KER and electron energy spectrum in Ne_2 fragmentation, the obtained energy resolution was 0.6 eV [39].

In Fig. 2, we display a coincident time-of-flight map, where TOF1 and TOF2 represent the flight times of the first and second detected ions, respectively. Two coincident islands marked by arrows A and B are observed, representing the Ar^+/CH_4^+ ion pair and Ar^+/CH_3^+ ion pair, respectively. The diagonal line in channel A indicates that the Ar^+ ion and the CH_4^+ ion are flying back to back, which is a signature of the two-body Coulomb explosion of the doubly charged $ArCH_4$ ion. For channel B, even though one H atom is lost, the diagonal line is still observed, suggesting that the H atom carries little momentum and does not substantially disturb the motion of the Ar^+ and CH_3^+ ions. In the following discussion, we will demonstrate that both channel A and channel B arise from ICD.

We chose the events in the Ar^+/CH_4^+ channel to reconstruct its kinetic energy release (KER) distribution. As shown by the blue solid squares in Fig. 3(a), only one peak with a maximum at 3.4 eV is observed. According to the classical reflection approximation $\mathrm{KER} \propto (Z_1 Z_2)/R$ [42], where Z_1, Z_2, and R denote the charge of the first and second detected ions, and the distance between the two ions at the instant of Coulomb explosion, respectively, we can deduce that the Coulomb explosion begins at a distance of 4.2 Å, which is the same as the equilibrium internuclear distance of the $ArCH_4$ dimer with Ar approaching the vertex of the CH_4 tetrahedron [43,44]. Therefore, it is a fast fragmentation

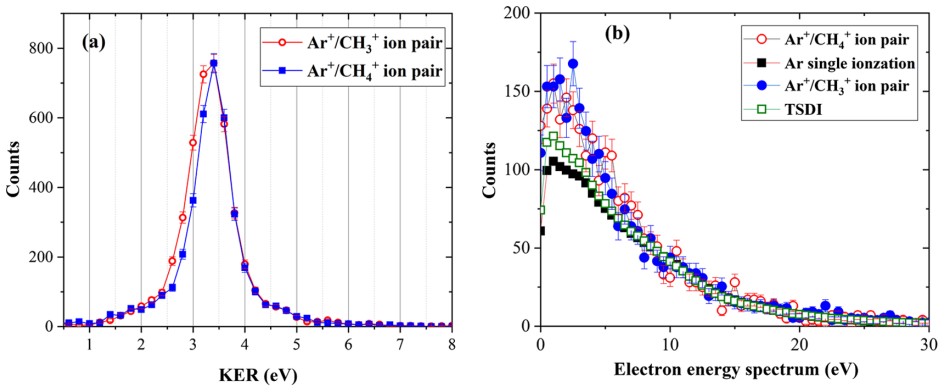

FIG. 3. (a) KER distribution of CH_4^+/Ar^+ ion pair (blue solid square) and KE-B distribution of the CH_3^+/Ar^+ ion pair (red open circle). (b) Electron energy spectrums to Ar^+/CH_4^+ ion pair (blue solid circle), CH_3^+/Ar^+ ion pair (red open circle), TSDI (green open square), and single ionization of Ar (black solid square). Note, for channel *A*, one electron is detected in coincidence with the Ar^+/CH_4^+ ion pair. For channel *B*, one electron is detected in coincidence with the Ar^+/CH_3^+ ion pair. For the Ar (e, 2e) reaction, one electron is detected in coincidence with the Ar^+ ion.

process, where the nuclear motion is negligible. Considering that the fast ICD mechanism has a typical lifetime in the femtosecond timescale [9], much shorter than the vibrational period of the cluster ion, it is a candidate for forming channel *A*. Namely, the simultaneous ionization and excitation state of Ar is first populated, forming the Ar^{+*}-CH_4 parent ion, then transfers energy to CH_4 and induces its ionization. A small part of events from a competition process named two-site double ionization (TSDI) will also be involved in our experiment, where the projectile electron ionizes the Ar atom and the CH_4 molecule sequentially. Its KER distribution is similar to that of the ICD process; for more details see the Supplemental Material [45].

In order to provide further evidence of ICD in channel *A*, the electron energy spectrum (EES) of channel *A* is shown in Fig. 3(b) by the blue solid circles. This spectrum involves the contributions of the ICD electron in Fig. 1(b), the emitted electron of Ar single ionization in Fig. 1(a), and electrons of TSDI. The EESs of the two later sources are shown by black solid squares and green open squares in Fig. 3(b), respectively; for more details see the Supplemental Material [45]. By normalizing these three curves in the energy range from 15 to 20 eV, as shown in Fig. 3(b), we observe an enhancement of low-energy electron yield in channel *A* whether compared to the TSDI case or the Ar single ionization case. This enhancement is consistent with the expectation of the ICD electron, as the minimum energy deposition needed to form the CH_4^+/Ar^+ ion pair with the KER of 3.4 eV is about 32 eV, while the most populated ionization-excitation states of $Ar^{+*}(3p^4nl)$ are lower than 43 eV [50], if ICD occurs, the excess energy (<11 eV) will cause the ICD electron to be located in the low energy region.

One may argue that the simultaneous ionization and excitation of CH_4, forming the CH_4^+-Ar parent ion, could also transfer energy to Ar and induce its ionization, contributing to channel *A*. However, this decay pathway can be excluded for the following reasons. The deposition energy needed to trigger ICD is about 32 eV, which will populate the CH_4^+ ion into a high-excitation state consisting of one electron in a Rydberg state and a doubly ionized core CH_4^{2+}. This ion core will separate into two singly charged fragments instantly, with one fragment capturing the excited electron and being neutralized, while the other escapes as an ion [51]. The excess energy is released through molecular Coulomb explosion, rather than being transferred to Ar, thus quenching ICD. We believe that the ICD due to the ionization of CH_4 is only a minor contribution compared to that of Ar ionization. The complete reaction of channel *A* can be described as follows: in the first step, an excitation and ionization state of Ar is populated by electron impact [Fig. 1(a)], and the second step is the ICD process transferring the excess energy from deexcitation to the neighboring CH_4 and inducing its ionization [Fig. 1(b)]. The third step is the Coulomb explosion between the two charged ions [Fig. 1(c)].

Now we turn to the discussion of channel *B*, which induces the dissociative ionization of CH_4 to CH_3^+/H. ICD is a possible explanation of the dissociative ionization of CH_4 to CH_3^+/H in channel *B*, as the energy deposition for both CH_4^+ ion and CH_3^+ ion originates from $1t_2$ electron ionization [52]. For soft (e, 2e) collisions with depositing energy around 13.7 eV, the produced CH_4^+ ion is in the vibrational ground state of $1t_2^{-1}$ and remains stable [52]. Alternatively, for slightly harder collisions with energy deposition more than about 1–1.5 eV, the CH_4^+ vibrational mode of $1t_2^{-1}$ is excited, and it dissociates into CH_3^+ and H in femtosecond timescale [51]. Considering the small energy difference between the vibrational ground state and the vibrationally excited states of CH_4^+, energy transfer via ICD may populate all these states. Then, the CH_4^+

corresponding to the former case contributes to channel A, while the CH_4^+ generated from the latter case evolves into CH_3^+ and H, contributing to channel B. If this scheme is true, the obtained KER and EES of channel B will be similar to that of channel A, since the two channels release similar excess energy, and the Coulomb explosion occurs at the same internuclear distance.

In order to confirm the above idea, the EES of channel B was reconstructed [see the red open circles in Fig. 3(b)]. By normalizing the EES of channel B to that of channel A in the energy area from 15–20 eV, we found that the shapes of the two curves are consistent with each other, as shown in Fig. 3(b). In addition, compared with the single ionization of the Ar atom and TSDI, an enhancement appears in the low-energy region, which is also in line with the expectation of ICD in channel B.

We reconstructed the kinetic energy of Ar^+ and CH_3^+ ions in channel B, and deduced their kinetic energy sum (KE-B), which approximately represents the KER of channel B (sum of kinetic energy of Ar^+, CH_3^+, and H). Because the dissociation energy of CH_4^+ to CH_3^+/H is 0.12 eV, which is 30 times smaller than that of the Coulomb explosion energy between Ar^+ and CH_4^+, we can ignore the influence of H to KER in the first approximation. As shown by the red open circles in Fig. 3(a), the KE-B overall shape of channel B agrees with the KER of channel A.

The similarities in both EESs and KERs (KE-B) between the two channels agree with the expectation of ICD, and suggest that ICD induces not only a fast fragmentation of $ArCH_4$ from its equilibrium internuclear distance and emission of low-energy ICD electrons, but also ionization dissociation of the CH_4^+ ion into CH_3^+ and H, as shown in the last step of Fig. 1(d).

Note that the KE-B distribution of channel B exhibits a slight broadening towards the low-energy side compared with the KER spectrum of channel A, as shown in Fig. 3(a). This broadening is a result of the time it takes for CH_4^+ to dissociate into H and CH_3^+. If the H atom loss takes place before Coulomb explosion in Fig. 3(c) ($t \leq 0$), the deduced KE-B distribution should be the same as the KER distribution of channel A, since all Coulomb repulsive potential is converted into the kinetic energy of CH_3^+ and Ar^+ ions. On the other hand, if the H loss occurs after the starting time of Coulomb explosion ($t > 0$), the H atom will take away some kinetic energy, inducing the shift of KE-B to the low-energy side.

We performed a classical simulation to deduce the KE-B as a function of the time t. In the simulation, we assumed that the Coulomb explosion between Ar^+ and CH_4^+ begins at time zero from a fixed internuclear distance of 4.2 Å. The H atom loss occurs at the time of t ($t > 0$), and the rest of Coulomb potential converts into the kinetic energy of the Ar^+-CH_3^+ ion pair. Additional details can be found in the Supplemental Material [45]. The classical simulation in

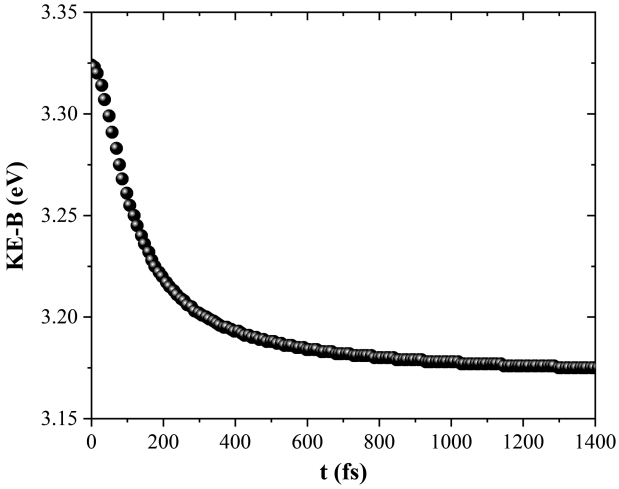

FIG. 4. The correlation between KE-B of CH_3^+-Ar^+ ion pair and H loss time t.

Fig. 4 shows that the KE-B value decreases monotonically with increasing time t, as the dissociated H atom takes away some Coulomb potential energy. When $t > 500$ fs, the KE-B approaches its asymptotic value, with an energy shift of 0.15 eV compared with the maximum at $t = 0$ fs. This simulation confirms that the dissociated H atom indeed takes away some Coulomb potential energy, and qualitatively explains the energy difference between KE-B and KER in Fig. 3(a).

Finally, we compared the count ratio of channel A to channel B in Fig. 2 and found that this ratio is 1.7, this value is larger than the yield ratio of CH_3^+ to CH_4^+ in the isolated CH_4 (e, 2e) case, whose reaction products are simultaneously measured in our experiment and the obtained count ratio is 1. First, this phenomenon suggests that ICD is more efficient than direct electron collision in populating the vibrationally excited states of CH_4^+. Second, as we mentioned in the introduction, an antenna-receiver complex could be developed via ICD, which enhances the ionization cross section of one atom (molecule) by a factor of at least 60 [18,19]. Following this idea, the higher intensity of channel B than channel A observed here tells us that the ICD mechanism can be used to enhance the cross section of molecular ionization dissociation with high efficiency, agreeing with previously theoretical predictions [36,37].

In conclusion, we conducted an electron impact fragmentation experiment of the $ArCH_4$ dimer to investigate molecular dissociation by interatomic or intermolecular energy transfer. By detecting one electron and two ions in coincidence, we demonstrated that the Ar^+/CH_4^+ ion pair arises from ICD. Our analysis of the Ar^+/CH_3^+ ion pair revealed that ICD triggers ionization dissociation of CH_4, where, after Ar is simultaneously ionized and excited, the excess energy is transferred to CH_4, populating the CH_4^+ into excited vibrational states. Subsequently, the molecular ion dissociates into the CH_3^+ and H ion pair. We further

found that the yield of this new decay channel is 1.7 times larger than the intensity of pure ionization by ICD, suggesting that this mechanism could be used to enhance the molecular ionization dissociation cross section with high efficiency. These findings not only contribute to a better understanding of ICD, but also offer a novel approach to directly trigger the ionization dissociation of covalent bonds in DNA molecules, surpassing the processes involving DEA. To activate this new channel in other molecule-atom systems, it is crucial for the ionization dissociation state of the acceptor molecule to be significantly lower than the ionization-excitation state of the donor atom. This condition can be satisfied in general rare gas-organic molecule complexes, as the appearance energy of most organic molecular dissociation-ionization states is below 20 eV, while lots of excitation-ionization states of rare gas can exist above 40 eV. One should note that this new pathway will be more efficient in the x-ray impact experiment, since the x-ray photon has a significantly larger absorption cross section for resonant-excitation states [33,34]. Further studies are needed to investigate the mechanism of this new channel in biomolecules and explore its potential applications in various fields, such as biochemistry and astrochemistry.

We acknowledge Tao Yang and Chen Liang for their helpful discussions. The work was supported by the National Key Research and Development Program of China under Grant No. 2022YFA1602500, Strategic Priority Research Program of the Chinese Academy of Sciences (XDB34020000), and the National Natural Science Foundation of China (NSFC) under Grants No. 11934004 and No. U1832201, Many thanks are given to the engineers who operated the HIRFL complex.

*Corresponding author: x.ma@impcas.ac.cn

[1] L. S. Cederbaum, J. Zobeley, and F. Tarantelli, Phys. Rev. Lett. **79**, 4778 (1997).
[2] T. Jahnke, A. Czasch, M. S. Schöffler, S. Schössler, A. Knapp, M. Käsz, J. Titze, C. Wimmer, K. Kreidi, R. E. Grisenti, A. Staudte, O. Jagutzki, U. Hergenhahn, H. Schmidt-Böcking, and R. Dörner, Phys. Rev. Lett. **93**, 163401 (2004).
[3] S. Marburger, O. Kugeler, U. Hergenhahn, and T. Möller, Phys. Rev. Lett. **90**, 203401 (2003).
[4] K. Sakai, S. Stoychev, T. Ouchi, I. Higuchi, M. Schöffler, T. Mazza, H. Fukuzawa, K. Nagaya, M. Yao, Y. Tamenori, A. I. Kuleff, N. Saito, and K. Ueda, Phys. Rev. Lett. **106**, 033401 (2011).
[5] W. Iskandar, J. Matsumoto, A. Leredde, X. Fléchard, B. Gervais, S. Guillous, D. Hennecart, A. Méry, J. Rangama, C. L. Zhou, H. Shiromaru, and A. Cassimi, Phys. Rev. Lett. **114**, 033201 (2015).
[6] H. K. Kim *et al.*, Proc. Natl. Acad. Sci. U.S.A. **108**, 11821 (2011).
[7] T. Havermeier, T. Jahnke, K. Kreidi, R. Wallauer, S. Voss, M. Schöffler, S. Schössler, L. Foucar, N. Neumann, J. Titze, H. Sann, M. Kühnel, J. Voigtsberger, J. H. Morilla, W. Schöllkopf, H. Schmidt-Böcking, R. E. Grisenti, and R. Dörner, Phys. Rev. Lett. **104**, 133401 (2010).
[8] N. Sisourat, N. V. Kryzhevoi, P. Kolorenc, S. Scheit, T. Jahnke, and L. S. Cederbaum, Nat. Phys. **6**, 508 (2010).
[9] K. Schnorr *et al.*, Phys. Rev. Lett. **111**, 093402 (2013).
[10] J. Zobeley, R. Santra, and L. S. Cederbaum, J. Chem. Phys. **115**, 5076 (2001).
[11] D. You *et al.*, Nat. Commun. **8**, 14277 (2017).
[12] I. Unger, R. Seidel, S. Thürmer, M. N. Pohl, E. F. Aziz, L. S. Cederbaum, E. Muchová, P. Slavíček, B. Winter, and N. V. Kryzhevoi, Nat. Chem. **9**, 708 (2017).
[13] J. Matsumoto, A. Leredde, X. Flechard, K. Hayakawa, H. Shiromaru, J. Rangama, C. L. Zhou, S. Guillous, D. Hennecart, T. Muranaka, A. Mery, B. Gervais, and A. Cassimi, Phys. Rev. Lett. **105**, 263202 (2010).
[14] A. Hans, V. Stumpf, X. Holzapfel, F. Wiegandt, P. Schmidt, C. Ozga, P. Reiß, L. B. Ltaief, C. Küstner-Wetekam, T. Jahnke, A. Ehresmann, P. V. Demekhin, K. Gokhberg, and A. Knie, New J. Phys. **20**, 012001 (2018).
[15] A. Hans, T. Miteva, X. Holzapfel, C. Ozga, P. Schmidt, H. Otto, G. Hartmann, C. Richter, N. Sisourat, A. Ehresmann, K. Gokhberg, U. Hergenhahn, and A. Knie, Phys. Rev. Lett. **123**, 213001 (2019).
[16] T. Jahnke, J. Phys. B **48**, 082001 (2015).
[17] T. Jahnke, U. Hergenhahn, B. Winter, R. Dörner, U. Frühling, P. V. Demekhin, K. Gokhberg, L. S. Cederbaum, A. Ehresmann, André Knie, and A. Dreuw, Chem. Rev. **120**, 11295 (2020).
[18] B. Najjari, A. B. Voitkiv, and C. Müller, Phys. Rev. Lett. **105**, 153002 (2010).
[19] F. Trinter *et al.*, Phys. Rev. Lett. **111**, 233004 (2013).
[20] V. Stumpf, P. Kolorenč, K. Gokhberg, and L. S. Cederbaum, Phys. Rev. Lett. **110**, 258302 (2013).
[21] A. C. LaForge, V. Stumpf, K. Gokhberg, J. von Vangerow, F. Stienkemeier, N. V. Kryzhevoi, P. O'Keeffe, A. Ciavardini, S. R. Krishnan, M. Coreno, K. C. Prince, R. Richter, R. Moshammer, T. Pfeifer, L. S. Cederbaum, and M. Mudrich, Phys. Rev. Lett. **116**, 203001 (2016).
[22] A. C. LaForge, M. Shcherbinin, F. Stienkemeier, R. Richter, R. Moshammer, T. Pfeifer, and M. Mudrich, Nat. Phys. **15**, 247 (2019).
[23] B. Boudaiffa, P. Cloutier, D. Hunting, M. A. Huels, and L. Sanche, Science **287**, 1658 (2000).
[24] É. Brun, P. Cloutier, C. Sicard-Roselli, M. Fromm, and L. Sanche, J. Phys. Chem. B **113**, 10008 (2009).
[25] E. Alizadeh, T. M. Orlando, and L. Sanche, Annu. Rev. Phys. Chem. **66**, 379 (2015).
[26] U. Hergenhahn, Int. J. Radiat. Biol. **88**, 871 (2012).
[27] S. D. Stoychev, A. I. Kuleff, and L. S. Cederbaum, J. Am. Chem. Soc. **133**, 6817 (2011).
[28] M. Mucke, M. Braune, S. Barth, M. Förstel, T. Li, V. Ulrich, T. Arion, U. Becker, A. Bradshaw, and U. Hergenhahn, Nat. Phys. **6**, 143 (2010).
[29] T. Jahnke, H. Sann, T. Havermeier, K. Kreidi, C. Stuck, M. Meckel, M. Schöffler, N. Neumann, R. Wallauer, S. Voss *et al.*, Nat. Phys. **6**, 139 (2010).
[30] X. Ren, E. Wang, A. D. Skitnevskaya, A. B. Trofimov, K. Gokhberg, and A. Dorn, Nat. Phys. **14**, 1062 (2018).

[31] X. Ren, J. Zhou, E. Wang, T. Yang, Z. Xu, N. Sisourat, T. Pfeifer, and A. Dorn, Nat. Chem. **14**, 232 (2022).
[32] V. Stumpf, K. Gokhberg, and L. S. Cederbaum, Nat. Chem. **8**, 237 (2016).
[33] K. Gokhberg, P. Kolorenč, I. Kuleff, and L. S. Cederbaum, Nature (London) **505**, 661 (2014).
[34] F. Trinter, M. S. Schöffler, H. K. Kim, F. P. Sturm, K. Cole, N. Neumann, A. Vredenborg, J. Williams, I. Bocharova, R. Guillemin, M. Simon, A. Belkacem, A. L. Landers, Th. Weber, H. Schmidt-Böcking, R. Dörner, and T. Jahnke, Nature (London) **505**, 664 (2014).
[35] P. O'Keeffe, E. Ripani, P. Bolognesi, M. Coreno, M. Devetta, C. Callegari, M. D. Fraia, K. C. Prince, R. Richter, M. Alagia, A. Kivimäk, and L. Avaldi, J. Phys. Chem. Lett. **4**, 1797 (2013).
[36] L. S. Cederbaum, J. Phys. Chem. Lett. **11**, 8964 (2020).
[37] Y. C. Chiang, S. Engin, P. Bao, F. Otto, P. Kolorenč, P. Votavová, T. Miteva, J. Gao, and N. Sisourat, Phys. Rev. A **100**, 052701 (2019).
[38] S. Yan, X. L. Zhu, S. F. Zhang, D. M. Zhao, P. Zhang, B. Wei, and X. Ma, Phys. Rev. A **102**, 032809 (2020).
[39] S. Yan, P. Zhang, V. Stumpf, K. Gokhberg, X. C. Zhang, S. Xu, B. Li, L. L. Shen, X. L. Zhu, W. T. Feng, S. F. Zhang, D. M. Zhao, and X. Ma, Phys. Rev. A **97**, 010701(R) (2018).
[40] R. Dörner, V. Mergel, O. Jagutzki, L. Spielberger, J. Ullrich, R. Moshammer, and H. Schmidt-Böcking, Phys. Rep. **330**, 95 (2000).
[41] J. Ullrich, R. Moshammer, A. Dorn, R. Dörner, L. Ph. H. Schmidt, and H. Schmidt-Böcking, Rep. Prog. Phys. **66**, 1463 (2003).
[42] E. A. Gislason, J. Chem. Phys. **58**, 3702 (1973).
[43] T. G. Heijmen, T. Korona, R. Moszynski, P. E. Wormer, and A. van der Avoird, J. Chem. Phys. **107**, 902 (1997).
[44] W. A. Alexander and D. Troya, J. Phys. Chem. A **110**, 10834 (2006).
[45] See Supplemental Material at http://link.aps.org/supplemental/10.1103/PhysRevLett.131.253001 for details about the analysis of the experimental result, the reconstruction of EES of TSDI, and the classical simulation of H loss from the CH_4^+ ion, which includes Refs. [46–49].
[46] S. Yan, P. Zhang, X. Ma, S. Xu, B. Li, X. L. Zhu, W. T. Feng, S. F. Zhang, D. M. Zhao, R. T. Zhang, D. L. Guo, and H. P. Liu, Phys. Rev. A **88**, 042712 (2013).
[47] H. C. Straub, P. Renault, B. G. Lindsay, K. A. Smith, and R. F. Stebbings, Phys. Rev. A **52**, 1115 (1995).
[48] M. J. Brunger, I. E. McCarthy, and E. Weigold, Phys. Rev. A **59**, 1245 (1999).
[49] G. P. Li, T. Takayanagi, K. Wakiya, and H. Suzuki, Phys. Rev. A **38**, 1831 (1988).
[50] X. Ren, T. Miteva, P. Kolorenč, K. Gokhberg, A. I. Kuleff, L. S. Cederbaum, and A. Dorn, Phys. Rev. A **96**, 032715 (2017).
[51] T. A. Field and J. H. Eland, J. Electron Spectrosc. Relat. Phenom. **73**, 209 (1995).
[52] S. Xu, X. Ma, X. Ren, A. Senftleben, T. Pflüger, S. Yan, P. Zhang, J. Yang, J. Ullrich, and A. Dorn, J. Chem. Phys. **138**, 134307 (2013).